UKACC International Conference on Control 2012
Cardiff, UK, 3-5 September 2012

Modelling Channel Flow over Riblets: Calculating the Energy Amplification

Aditya Kasliwal, Stephen Duncan and Antonis Papachristodoulou

Abstract— **Riblets have been considered as a passive method for drag reduction. Riblets are structures on a surface that run parallel to one another, which are aligned longitudinally to the flow. It has been shown experimentally that when the shape, spacing and height of the riblets are optimized, the drag coefficient over the surface can be reduced by up to 10%. These results have also been confirmed by direct numerical simulation studies. Although the benefits of riblets have been known since the early 1980's, the mechanism of drag reduction is still not fully understood. This paper examines the effect of riblet structures on the amplification of background noise within channel flow between two parallel plates (Poiseuille flow), where riblets are present on the surface of one of the plates. A linearized version of the Navier-Stokes equation about the steady flow is developed and through a coordinate transformation, the boundary conditions associated with the riblets are transferred into the partial differential equations. Previous work has used spectral methods to discretize these equations, leading to a large-scale state space model, and the energy amplification was calculated for the streamwise constant component of the flow from the controllability gramian. However, solving the associated Lyapunov equation can be computationally prohibitive, which limits the density of the discretized grid. This paper shows how the problem can be transformed to decouple the system, so that the gramian can be obtained by solving a set of smaller Lyapunov equations, which has the potential to allow the energy amplification to be calculated for systems with a dense discretization grid.**

Index Terms— **Fluid flow, drag reduction, Lyapunov equation, energy amplification, riblets**

I. Introduction

One approach that has been considered in the past that results in a significant reduction in the drag caused by a fluid flowing past a body is the introduction of riblet structures on the surface of the body [1], [2], [3]. Riblets are structures that run parallel to one another, that are positioned longitudinally to the flow and usually have a triangular cross-section in the transverse direction. By contrast with approaches such as suction/blow mechanisms, riblets can be regarded as a passive drag reduction mechanism [4]. Previous research has shown that riblet structures can be optimized to produce a reduction in the drag coefficient of up to 10% [2]. It is believed that the mechanism responsible for this level of drag reduction is the interaction of the riblets with the structure of the boundary layer, which leads to a reduction in drag, despite the significant increase in the area of the modified surface that is in contact with the flow compared to a smooth surface. This drag-reduction mechanism is observed widely in nature, for example on shark skin and scallop shells [5], [6]. Static riblet structures (often in the form of films that cover the surface) have been used in a number of fields and in the 1990's tests on a scale model of an Airbus A320 cruising at Mach 0.7 have shown reductions in viscous drag of 4.85% [7], [8]. However, despite these benefits, there has not as yet been a satisfactory explanation for the mechanism of drag reduction using riblet structures. Experimental and Computational Fluid Dynamics (CFD) studies have suggested that riblets induce streamwise vortices that sit within the riblets [9], [10], although recent work has shown that riblets induce spanwise vortices close to the riblet surface and it is these that change the drag over the surface [11], [12].

The results presented here build on previous work [13], [14] that combines ideas from control theory and aerodynamics, by extending an existing direct numerical simulation of the flow between two parallel plates (Poiseulle flow), where riblets are present on the surface of one of the plates. The model uses concepts from linear control theory to determine the transient growth of background noise energy amplification in the linearized Navier-Stokes equations [15], [16]. We investigate how the transient growth in energy alters with the introduction of riblet structures by using the model to predict how the shape and positioning of the riblets affect this transient energy growth. The model calculates the amplification of background noise energy, together with the drag on the surface of the plates, for a given riblet geometry, by using a transformation of coordinates that will 'passes' the non-uniformity of the boundary associated with the riblet structure on one of the walls, into the equations of motion. Once this equation is obtained, a numerical model is developed using a Chebyshev discretization approach in the wall-normal direction and a Fourier representation in the streamwise and spanwise directions and estimates of the reduction in energy amplification are obtained as a function of different geometries. Previous work [13], [14] has modelled the flow at relatively low Reynolds numbers due to the computational complexity of the problem, because in order to find the energy amplification, it was necessary to solve a high dimension Lyapunov equation, which is a computationally intensive step. However, by exploiting the inherent structure of the problem that is associated with the Fourier representation in the spanwise direction, it is possible to decompose the problem into a set of decoupled Lyapunov equations of lower dimension. This has the potential to allow the flow to be modelled at higher Reynolds numbers and reduced riblet spacing that require denser discretization grids, which is where the benefits of the riblets structures are

A. Kasliwal, S. Duncan and A. Papachristodoulou are with the Department of Engineering Science, University of Oxford, Parks Road, Oxford, OX1 3PJ, United Kingdom. Emails aditya.kasliwal@mansfield.ox.ac.uk, stephen.duncan@eng.ox.ac.uk, antonis@eng.ox.ac.uk

978-1-4673-1558-6/12/$31.00 ©2012 IEEE

observed. It will also allow comparison with experimental results and with CFD simulations that have been reported in the literature.

The paper is organized as follows. Section II develops the equations describing the channel flow and uses a coordinate transformation to convert the boundary conditions associated with the riblet structures into a uniform domain. In Section III, the equations describing the linearized flow about the steady flow are derived. Section IV shows how Fourier methods can be used to create a large-scale, finite-dimensional state space model and describes how the structure of the model can be exploited to calculate the amplification of the energy associated with background noise in a computationally efficient manner. Section V gives the results for the effect on the energy amplification of introducing riblets for a specific flow regime and Section VI concludes the paper.

II. Transforming the Equations of Motion

We consider channel flow between two stationary plates with the geometry of the problem as shown in Fig. 1, where $\tilde{x}$, $\tilde{y}$ and $\tilde{z}$ are the coordinates of the streamwise, wall-normal and spanwise directions, respectively. The upper wall is a flat plate, while the lower wall is a plate with riblets aligned with the streamwise direction. The dimensions of the problem are normalized, so that the upper boundary of the flow occurs at the plate positioned at $\tilde{y} = 1$, while the lower boundary is at

$$\tilde{y} = -1 + f(\tilde{z}) \tag{1}$$

where $f(\tilde{z})$ describes the "shape" of the riblets. The analysis will be restricted to riblets that are aligned with the streamwise direction and are independent of $\tilde{x}$.

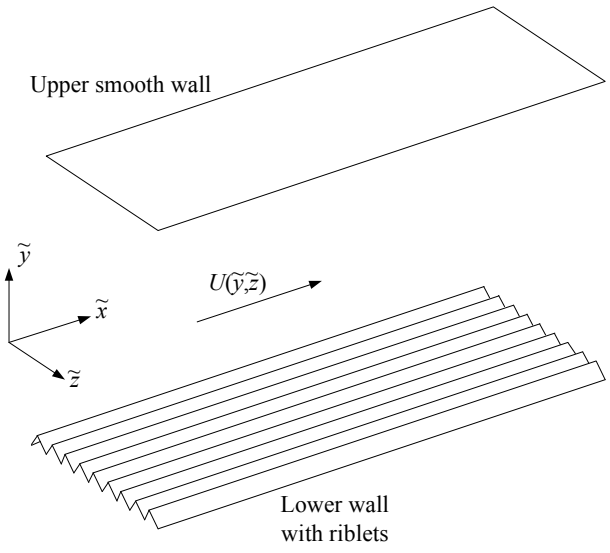

Fig. 1. Three-dimensional view of computational domain showing riblet structure on lower wall of channel. $U(\tilde{y}, \tilde{z})$ denotes the direction of the steady, streamwise flow.

The streamwise, wall-normal and span-wise components of the flow in the coordinate system $(\tilde{x}, \tilde{y}, \tilde{z})$ are denoted by $u(\tilde{x}, \tilde{y}, \tilde{z}, t)$, $v(\tilde{x}, \tilde{y}, \tilde{z}, t)$ and $w(\tilde{x}, \tilde{y}, \tilde{z}, t)$ respectively, and the non-dimensionalised Navier-Stokes equations in this coordinate system are given by

$$\left(\frac{\partial}{\partial t} + u\frac{\partial}{\partial \tilde{x}} + v\frac{\partial}{\partial \tilde{y}} + w\frac{\partial}{\partial \tilde{z}}\right) u = -\frac{\partial p}{\partial \tilde{x}} + \frac{1}{\mathrm{Re}}\tilde{\Delta} u \tag{2}$$

$$\left(\frac{\partial}{\partial t} + u\frac{\partial}{\partial \tilde{x}} + v\frac{\partial}{\partial \tilde{y}} + w\frac{\partial}{\partial \tilde{z}}\right) v = -\frac{\partial p}{\partial \tilde{y}} + \frac{1}{\mathrm{Re}}\tilde{\Delta} v \tag{3}$$

$$\left(\frac{\partial}{\partial t} + u\frac{\partial}{\partial \tilde{x}} + v\frac{\partial}{\partial \tilde{y}} + w\frac{\partial}{\partial \tilde{z}}\right) w = -\frac{\partial p}{\partial \tilde{z}} + \frac{1}{\mathrm{Re}}\tilde{\Delta} w \tag{4}$$

$$\frac{\partial u}{\partial \tilde{x}} + \frac{\partial v}{\partial \tilde{y}} + \frac{\partial w}{\partial \tilde{z}} = 0 \tag{5}$$

where p is the pressure, Re is the Reynolds number and

$$\tilde{\Delta} = \frac{\partial^2}{\partial \tilde{x}^2} + \frac{\partial^2}{\partial \tilde{y}^2} + \frac{\partial^2}{\partial \tilde{z}^2} \tag{6}$$

For the smooth wall at $\tilde{y} = 1$, the boundary conditions are

$$u(\tilde{x}, 1, \tilde{z}) = v(\tilde{x}, 1, \tilde{z}) = w(\tilde{x}, 1, \tilde{z}) = 0 \tag{7}$$

together with

$$\left.\frac{\partial v}{\partial \tilde{y}}\right|_{\tilde{y}=1} = 0 \tag{8}$$

while for the riblet wall at $\tilde{y} = -1 + f(\tilde{z})$, the boundary conditions are

$$\begin{aligned} u(\tilde{x}, -1 + f(\tilde{z}), \tilde{z}) &= v(\tilde{x}, -1 + f(\tilde{z}), \tilde{z}) \\ &= w(\tilde{x}, -1 + f(\tilde{z}), \tilde{z}) = 0 \end{aligned} \tag{9}$$

with

$$\left.\frac{\partial v}{\partial n}\right|_{\tilde{y}=-1+f(\tilde{z})} = 0 \tag{10}$$

where n is the normal to the surface of riblets.

We now apply a change of coordinates

$$\begin{aligned} x &= \tilde{x} \\ y &= F(\tilde{y}, \tilde{z}) \\ z &= \tilde{z} \end{aligned} \tag{11}$$

where

$$y = F(\tilde{y}, \tilde{z}) = \frac{2\tilde{y} - f(\tilde{z})}{2 - f(\tilde{z})} \tag{12}$$

which has the effect of mapping $\tilde{y} \in [-1 + f(\tilde{z}), 1]$ to $y \in [-1, 1]$.

The Navier-Stokes equations in the new coordinate system

then become [14]

$$\left(\frac{\partial}{\partial t}+u\frac{\partial}{\partial x}+v\frac{\partial F}{\partial \tilde{y}}\frac{\partial}{\partial y}+w\frac{\partial F}{\partial \tilde{z}}\frac{\partial}{\partial y}+w\frac{\partial}{\partial z}\right)u = -\frac{\partial p}{\partial x}+\frac{1}{\mathrm{Re}}\tilde{\Delta}u \quad (13)$$

$$\left(\frac{\partial}{\partial t}+u\frac{\partial}{\partial x}+v\frac{\partial F}{\partial \tilde{y}}\frac{\partial}{\partial y}+w\frac{\partial F}{\partial \tilde{z}}\frac{\partial}{\partial y}+w\frac{\partial}{\partial z}\right)v = -\frac{\partial F}{\partial \tilde{y}}\frac{\partial p}{\partial y}+\frac{1}{\mathrm{Re}}\tilde{\Delta}v \quad (14)$$

$$\left(\frac{\partial}{\partial t}+u\frac{\partial}{\partial x}+v\frac{\partial F}{\partial \tilde{y}}\frac{\partial}{\partial y}+w\frac{\partial F}{\partial \tilde{z}}\frac{\partial}{\partial y}+w\frac{\partial}{\partial z}\right)w = -\frac{\partial p}{\partial z}-\frac{\partial F}{\partial \tilde{z}}\frac{\partial p}{\partial y}+\frac{1}{\mathrm{Re}}\tilde{\Delta}w \quad (15)$$

$$\frac{\partial u}{\partial x}+\frac{\partial F}{\partial \tilde{y}}\frac{\partial v}{\partial y}+\frac{\partial F}{\partial \tilde{z}}\frac{\partial w}{\partial y}+\frac{\partial w}{\partial z}=0 \quad (16)$$

where

$$\tilde{\Delta} = \frac{\partial^2}{\partial x^2}+\left(\frac{\partial F}{\partial \tilde{y}}\right)^2\frac{\partial^2}{\partial y^2}+\left(\frac{\partial F}{\partial \tilde{z}}\right)^2\frac{\partial^2}{\partial y^2}+\frac{\partial^2}{\partial z^2} +\frac{\partial}{\partial \tilde{y}}\left(\frac{\partial F}{\partial \tilde{y}}\right)\frac{\partial}{\partial y}+\frac{\partial}{\partial \tilde{z}}\left(\frac{\partial F}{\partial \tilde{z}}\right)\frac{\partial}{\partial y}+2\frac{\partial F}{\partial \tilde{z}}\frac{\partial^2}{\partial y \partial z} \quad (17)$$

III. Linearized Equations

The steady state flow, $(U,0,0)$, satisfies

$$U\frac{\partial U}{\partial x} = -\frac{\partial P}{\partial x}+\frac{1}{\mathrm{Re}}\tilde{\Delta}U \quad (18)$$

$$0 = -\frac{\partial F}{\partial \tilde{y}}\frac{\partial P}{\partial y} \quad (19)$$

$$0 = -\frac{\partial P}{\partial z}-\frac{\partial F}{\partial \tilde{z}}\frac{\partial P}{\partial y} \quad (20)$$

$$\frac{\partial U}{\partial x} = 0 \quad (21)$$

Since we are restricting our attention to the case of straight riblets aligned with the streamwise direction, so that $f(\hat{z})$ does not depend upon $\hat{x}$, then $P=P(x)$ and $U=U(y,z)$, where $U(y,z)$ is the solution of

$$\tilde{\Delta}U=-2\mathrm{Re} \quad (22)$$

We now redefine the streamwise flow as $u(x,y,z,t)+U(y,z)$, where $u(x,y,z,t)$ denotes the flow *relative* to the solution of steady flow problem, $U(y,z)$, and the pressure as $p(x,y,z,t)+P(x)$, where $p(x,y,z,t)$ is the pressure *relative* to $P(x)$. Linearizing about this steady solution and applying the change of coordinates, the Navier-Stokes equations become

$$\left(\frac{\partial}{\partial t}+U\frac{\partial}{\partial \tilde{x}}\right)u+v\frac{\partial U}{\partial \tilde{y}}+w\frac{\partial U}{\partial \tilde{z}} = -\frac{\partial p}{\partial \tilde{x}}+\frac{1}{\mathrm{Re}}\tilde{\Delta}u \quad (23)$$

$$\left(\frac{\partial}{\partial t}+U\frac{\partial}{\partial \tilde{x}}\right)v = -\frac{\partial p}{\partial \tilde{y}}+\frac{1}{\mathrm{Re}}\tilde{\Delta}v \quad (24)$$

$$\left(\frac{\partial}{\partial t}+U\frac{\partial}{\partial \tilde{x}}\right)w = -\frac{\partial p}{\partial \tilde{z}}+\frac{1}{\mathrm{Re}}\tilde{\Delta}w \quad (25)$$

$$\frac{\partial u}{\partial \tilde{x}}+\frac{\partial v}{\partial \tilde{y}}+\frac{\partial w}{\partial \tilde{z}} = 0 \quad (26)$$

Introducing

$$\eta=\frac{\partial u}{\partial \tilde{z}}-\frac{\partial w}{\partial \tilde{x}} \quad (27)$$

and rearranging, we obtain

$$\left(\frac{\partial}{\partial t}+U\frac{\partial}{\partial \tilde{x}}\right)\eta - \frac{\partial U}{\partial \tilde{z}}\frac{\partial v}{\partial \tilde{y}}+\frac{\partial U}{\partial \tilde{y}}\frac{\partial v}{\partial \tilde{z}}+v\frac{\partial^2 U}{\partial \tilde{y}\partial \tilde{z}}+w\frac{\partial^2 U}{\partial \tilde{z}^2} = \frac{1}{\mathrm{Re}}\tilde{\Delta}\eta \quad (28)$$

The flow is now described by equations that depend upon v, η and w. To eliminate w, define

$$\eta=\frac{\partial u}{\partial \tilde{z}}-\frac{\partial w}{\partial \tilde{x}} \quad (29)$$

which leads to

$$w=-\left(\frac{\partial^2}{\partial \tilde{z}^2}+\frac{\partial^2}{\partial \tilde{x}^2}\right)^{-1}\left(\frac{\partial \eta}{\partial \tilde{x}}+\frac{\partial^2 v}{\partial \tilde{y}\partial \tilde{z}}\right) \quad (30)$$

We now assume that the flow is streamwise constant, so that v, η and w are independent of $\tilde{x}$, and $\frac{\partial}{\partial \tilde{x}}=\frac{\partial}{\partial x}=0$, and following some lengthy manipulations (details are given in [13], [14]), the linearized flow can be described by

$$\frac{\partial}{\partial t}\tilde{\Delta}v = \frac{1}{\mathrm{Re}}\tilde{\Delta}\tilde{\Delta}v \quad (31)$$

$$\frac{\partial}{\partial t}\eta = \tilde{\mathcal{C}}v+\frac{1}{\mathrm{Re}}\tilde{\Delta}\eta \quad (32)$$

where

$$\tilde{\mathcal{C}}=\frac{\partial U}{\partial \tilde{z}}\frac{\partial}{\partial \tilde{y}}-\frac{\partial U}{\partial \tilde{y}}\frac{\partial}{\partial \tilde{z}}-\frac{\partial^2 U}{\partial \tilde{y}\partial \tilde{z}}+\frac{\partial^2 U}{\partial \tilde{z}^2}\left(\frac{\partial^2}{\partial \tilde{z}^2}\right)^{-1}\frac{\partial^2}{\partial \tilde{y}\partial \tilde{z}} \quad (33)$$

IV. Representation in Spatial Fourier Domain

Using (17), the expression for $\tilde{\Delta}$ and $\tilde{\Delta}\tilde{\Delta}$ can be expressed in terms of the steady-state flow U and the partial differentials of $F(\tilde{y},\tilde{z})$. In order to obtain expressions for these operators, we require

$$y=F(\tilde{y},\tilde{z})=\frac{2\tilde{y}-f(\tilde{z})}{2-f(\tilde{z})} \quad (34)$$

and because $\tilde{z}=z$, then

$$\tilde{y}=y+\frac{f(z)}{2}(1-y) \quad (35)$$

so that

$$\frac{\partial F}{\partial \tilde{y}} = \frac{2}{2 - f(z)} \tag{36}$$

$$\frac{\partial F}{\partial \tilde{z}} = \frac{(y-1)\ f'(z)}{2 - f(z)} \tag{37}$$

where $f'(z)$ denotes the differential of $f(z)$ with respect to z. The higher partial derivatives of $F(\tilde{y}, \tilde{z})$ can also be derived, but the resulting expressions for the transformed operators are rather cumbersome and are omitted from this paper. Full details are given in [14].

The operator $\tilde{\Delta}$ can be written as

$$\tilde{\Delta} = K_1(y,z)\frac{\partial}{\partial y} + K_2(y,z)\frac{\partial^2}{\partial y \partial z} + K_3(y,z)\frac{\partial^2}{\partial y^2} + \frac{\partial^2}{\partial z^2} \tag{38}$$

with

$$K_1(y,z) = \frac{\partial}{\partial z}\left(\frac{\partial F}{\partial \tilde{z}}\right) + \frac{\partial F}{\partial \tilde{y}}\frac{\partial}{\partial y}\left(\frac{\partial F}{\partial \tilde{y}}\right) + \frac{\partial F}{\partial \tilde{z}}\frac{\partial}{\partial y}\left(\frac{\partial F}{\partial \tilde{z}}\right) \tag{39}$$

$$K_2(y,z) = 2\frac{\partial F}{\partial \tilde{z}} \tag{40}$$

$$K_3(y,z) = \left(\frac{\partial F}{\partial \tilde{y}}\right)^2 + \left(\frac{\partial F}{\partial \tilde{z}}\right)^2 \tag{41}$$

The operators in (31) and (32) depend upon the steady state profile $U(y,z)$. Because the flow is taken to be periodic in the $\tilde{z}$ direction with period 2π, and since $\tilde{z} = z$ then

$$U(y,z) = U(y, z + 2\pi) \tag{42}$$

the spanwise component of the flow can be approximated by a linear combination of Galerkin trial functions, $\mathrm{e}^{\mathrm{i}nz}$ for $n \in \mathbb{Z}$, so that

$$U(y,z) = \sum_{n=-\infty}^{\infty} \hat{U}_n(y)\mathrm{e}^{\mathrm{i}nz} \tag{43}$$

The riblet structure is also taken to be periodic in the $\tilde{z}$ (and z) direction, so that $f(z)$ can be expressed as

$$f(z) = \sum_{n=-\infty}^{\infty} \hat{f}_n \mathrm{e}^{\mathrm{i}nz} \tag{44}$$

However, assuming that there are an integer number of riblets, $P \in \mathbb{Z}^+$, in the region $z \in [0, 2\pi]$, then $\hat{f}_n = 0$ for all $n \neq mP$, where m is an integer. When the spacing between riblets is small, as is usually the case for flow with high Reynolds numbers, then P is large, which means that only coefficients $\hat{f}_n$ for values of n that are multiples of P are non-zero, and this sparsity is exploited in the solution of the problem.

The expression in (36) and (37) can be simplified by defining

$$g(z) = \frac{1}{2 - f(z)} \tag{45}$$

Expanding $g(z)$ as a linear combination of powers of $f(z)$

$$g(z) = \frac{1}{2 - f(z)} = \frac{1}{2}\left(1 + \frac{1}{2}f(z) + \frac{1}{4}[f(z)]^2 + \dots\right) \tag{46}$$

then this is periodic and can be expressed as

$$g(z) = \sum_{n=-\infty}^{\infty} \hat{g}_n \mathrm{e}^{\mathrm{i}nz} \tag{47}$$

where $\hat{g}_n = 0$ for all $n \neq mP$. Since the expressions in (36) and (37) and the higher derivatives are periodic, the terms $K_1(y,z)$, $K_2(y,z)$ and $K_3(y,z)$ can also be expressed in terms of Fourier series of the form

$$K_1(y,z) = \sum_{n=-\infty}^{\infty} \hat{k}_n^{(1)}(y)\,\mathrm{e}^{\mathrm{i}nz} \tag{48}$$

$$K_2(y,z) = \sum_{n=-\infty}^{\infty} \hat{k}_n^{(2)}(y)\,\mathrm{e}^{\mathrm{i}nz} \tag{49}$$

$$K_3(y,z) = \sum_{n=-\infty}^{\infty} \hat{k}_n^{(3)}(y)\,\mathrm{e}^{\mathrm{i}nz} \tag{50}$$

Because both $\hat{f}_n$ and $\hat{g}_n$ are non zero when n is an exact multiple of P, then this will also be true for the coefficients, $\hat{k}_n^{(1)}$, in these expansions.

Using these expansions in the flow equation (22) gives

$$\begin{aligned}
&\sum_{n=-\infty}^{\infty} \hat{k}_n^{(1)}(y)\,\mathrm{e}^{\mathrm{i}nz}\left(\frac{\partial}{\partial y}\sum_{m=-\infty}^{\infty}\hat{U}_m(y)\mathrm{e}^{\mathrm{i}mz}\right) \\
&\quad + \sum_{n=-\infty}^{\infty} \hat{k}_n^{(2)}(y)\,\mathrm{e}^{\mathrm{i}nz}\left(\frac{\partial^2}{\partial y \partial z}\sum_{m=-\infty}^{\infty}\hat{U}_m(y)\mathrm{e}^{\mathrm{i}mz}\right) \\
&\quad + \sum_{n=-\infty}^{\infty} \hat{k}_n^{(3)}(y)\,\mathrm{e}^{\mathrm{i}nz}\left(\frac{\partial^2}{\partial y^2}\sum_{m=-\infty}^{\infty}\hat{U}_m(y)\mathrm{e}^{\mathrm{i}mz}\right) \\
&\quad + \sum_{n=-\infty}^{\infty} \frac{\partial^2 \hat{U}_n(y)}{\partial z^2}\mathrm{e}^{\mathrm{i}nz} = -2\mathrm{Re}
\end{aligned} \tag{51}$$

Defining an inner product as

$$\langle p(y,z)q(y,z)\rangle = \int_0^{2\pi} \overline{p(y,z)}\, q(y,z)dz \tag{52}$$

then taking the inner product of the expression in (51) with a Galerkin trial function, $\mathrm{e}^{\mathrm{i}\ell z}$ and exploiting the orthogonality of the trial functions with respect to z

$$\begin{aligned}
2\pi \sum_{m=-\infty}^{\infty} \hat{k}_{\ell-m}^{(3)}(y)\frac{\mathrm{d}^2\hat{U}_m}{\mathrm{d}y^2} + \left[\hat{k}_{\ell-m}^{(1)}(y) + \mathrm{i}m\,\hat{k}_{\ell-m}^{(2)}(y)\right]\frac{\mathrm{d}\hat{U}_m}{\mathrm{d}y} \\
- m^2\hat{U}_m(y) = b_\ell \qquad \text{for } \ell \in \mathbb{Z}
\end{aligned} \tag{53}$$

where

$$b_\ell = \begin{cases} -4\pi\mathrm{Re} & \text{for} \quad \ell = 0 \\ 0 & \text{for} \quad \ell \neq 0 \end{cases} \tag{54}$$

If $U(y,z)$ is approximated by its projection onto a finite basis, then the summation is limited to $2M+1$ terms, and (53 reduces to $2M+1$ coupled second order, ordinary differential equations. The values of $\hat{U}_m(y)$ can be solved numerically at the Chebyshev points on $y \in [-1, 1]$ by stacking the values of $\hat{U}_m(y)$ at K sample points for each ℓ into a vector $\hat{\mathbf{U}} \in \mathbb{R}^{(2M+1)K}$, so that

$$\hat{\mathbf{U}} = \left[\ \hat{\mathbf{U}}_{-M}\ \dots\ \hat{\mathbf{U}}_{-1}\ \hat{\mathbf{U}}_0\ \hat{\mathbf{U}}_1\ \dots \hat{\mathbf{U}}_M\ \right]^{\mathrm{T}} \tag{55}$$

where $\hat{\mathbf{U}}_m \in \mathbb{R}^K$ are the samples of $U_m(y)$ at the K Chebyshev points [17], [18]. The discretised version of the coupled ODE's in (53) take the form

$$\mathbf{E}\hat{\mathbf{U}} = \mathbf{b} \tag{56}$$

where $\mathbf{b} \in \mathbb{C}^{(2M+1)K}$ contains the terms b_ℓ. The $\mathbf{E} \in \mathbb{C}^{(2M+1)K\times(2M+1)K}$ consists of a series of blocks $[\mathbf{E}]_{\ell,m} \in \mathbb{C}^{K\times K}$, that satisfy

$$[\mathbf{E}]_{\ell,m} = \text{diag}\left\{\hat{\mathbf{k}}^{(3)}_{\ell-m}\right\}\mathbf{D}_K^2 + \text{diag}\left\{\hat{\mathbf{k}}^{(1)}_{\ell-m} + \imath m\,\hat{\mathbf{k}}^{(2)}_{\ell-m}\right\}\mathbf{D}_K - \text{diag}\left\{m^2\right\} \tag{57}$$

where $\mathbf{D}_K \in \mathbb{R}^{K\times K}$ and $\mathbf{D}_K^2 \in \mathbb{R}^{K\times K}$ are the first and second Chebyshev differentiation matrices respectively, and $\hat{\mathbf{k}}^{(1)}_{\ell-m} \in \mathbb{C}^K$, $\hat{\mathbf{k}}^{(2)}_{\ell-m} \in \mathbb{C}^K$, $\hat{\mathbf{k}}^{(3)}_{\ell-m} \in \mathbb{C}^K$ and $\hat{\mathbf{k}}^{(4)}_{\ell-m} \in \mathbb{C}^K$ are vectors obtained by sampling $\hat{k}^{(1)}_{\ell-m}(y)$, $\hat{k}^{(2)}_{\ell-m}(y)$ and $\hat{k}^{(3)}_{\ell-m}(y)$ at the K Chebyshev points.

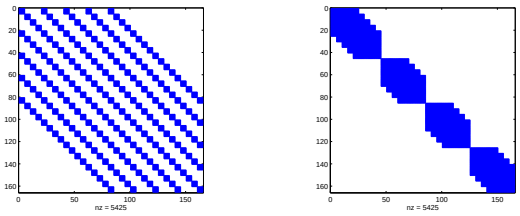

Fig. 2. Structure of $\mathbf{E}$ matrix (a) before reordering and (b) after reordering

The key point is that because $\hat{k}^{(1)}_{\ell-m}(y)$, $\hat{k}^{(2)}_{\ell-m}(y)$ and $\hat{k}^{(3)}_{\ell-m}(y)$ are only non zero when $\ell - m$ is an exact multiple of P, the $\mathbf{E}$ matrix has the structure shown in Figure 2(a), where each of the individual blocks has dimension K by K. By rearranging the order of the terms in $\hat{\mathbf{U}}$, the structure of the $\mathbf{E}$ matrix can be arranged into the block diagonal form shown in Figure 2(b), which consists of P blocks, each of dimension $[2(M/P)+1]K$ by $[2(M/P)+1]K$. This structure can be exploited to solve the overall problem as a set of P individual sub-problems, which has two advantages. Firstly, solving P smaller problems reduces the computational load by a factor of P, and secondly, the problem can be implemented as P sub-problems, which can be solved separately.

Remark 1. For the case shown in the Figure 2, the first block has dimension $[2(M/P)+1]K$ by $[2(M/P)+1]K$, but the subsequent blocks have dimension $2(M/P)K$ by $2(M/P)K$. This is a consequence of using $2M+1$ terms in the finite Galerkin expansion in (43). To ensure that all blocks are of equal size, it is necessary to restrict the expansion to $2M$ terms so that $m \in \{-M+1, \ldots, -1, 0, 1, \ldots, M\}$, although this makes the indexing of the matrices more complicated.

Remark 2. To solve the steady state problem, it is only necessary to solve the sub-problem associated with the first sub-block, because the elements of the $\mathbf{b}$ vector associated with the other sub-problems are all zero. However, this will not be the case when solving the full linearised problem.

The linearised equations for the flow in (31) and (32) can be expressed in terms of Fourier series for

$$v(y,z,t) = \sum_{n=-\infty}^{\infty} \hat{v}_n(y,t)\mathrm{e}^{\imath nz} \tag{58}$$

$$\eta(y,z,t) = \sum_{n=-\infty}^{\infty} \hat{\eta}_n(y,t)\mathrm{e}^{\imath nz} \tag{59}$$

We discretize the problem using a Chebyshev grid in the y direction, which reduces the differential operators in (31) and (32) to matrices [19]. Because of the orthogonality of the Galerkin approximation in the z direction, the problem is reduced to a decoupled set of state space models of the form (the procedure is the exactly the same as in the derivation of (57) for the steady state solution, although the expressions are cumbersome, so details are given in [20])

$$\frac{d}{dt}\begin{bmatrix}\hat{\mathbf{v}}_\ell \\ \hat{\eta}_\ell\end{bmatrix} = \begin{bmatrix}\hat{\mathbf{L}}^\ell_{11} & \mathbf{0} \\ \hat{\mathbf{L}}^\ell_{21} & \hat{\mathbf{L}}^\ell_{22}\end{bmatrix}\begin{bmatrix}\hat{\mathbf{v}}_\ell \\ \hat{\eta}_\ell\end{bmatrix} \tag{60}$$

where $\hat{\mathbf{L}}^\ell_{11}$, $\hat{\mathbf{L}}^\ell_{21}$ and $\hat{\mathbf{L}}^\ell_{22}$ are the matrices obtained by discretizing the operators for each Fourier coefficient. The states are not functions of the streamwise position x as it is assumed that the flow is streamwise constant.

The amplification of the energy at the output of the system resulting from the addition of Gaussian white noise at each sampling position in the Chebyshev grid can be found by solving the Lyapunov equation to find the controllability gramian, $\hat{\mathbf{X}}^\ell$ of the (discretized) system associated with each Fourier mode

$$\hat{\mathbf{A}}^\ell\hat{\mathbf{X}}^\ell + \hat{\mathbf{X}}^\ell\hat{\mathbf{A}}^{\ell\,\mathrm{T}} + \hat{\mathbf{Q}}^\ell = 0 \tag{61}$$

where $\mathbf{A}$ matrix is block diagonal

$$\hat{\mathbf{A}}^\ell = \begin{bmatrix}\hat{\mathbf{L}}^\ell_{11} & \mathbf{0} \\ \hat{\mathbf{L}}^\ell_{12} & \hat{\mathbf{L}}^\ell_{22}\end{bmatrix} \tag{62}$$

and $\hat{\mathbf{Q}}^\ell$ is the covariance matrix of the white noise, which has the structure

$$\hat{\mathbf{Q}}^\ell = \begin{bmatrix}\hat{\mathbf{Q}}^\ell_{11} & \mathbf{0} \\ \mathbf{0} & \hat{\mathbf{Q}}^\ell_{22}\end{bmatrix} \tag{63}$$

where $\hat{\mathbf{Q}}^\ell_{11}$ and $\hat{\mathbf{Q}}^\ell_{22}$ are diagonal. The structure of the problem can be exploited to break it into three separate equations [15], each of which can be solved efficiently using Cholesky factorizations [14].

The total amplification of the noise energy is given by the trace of $\mathbf{C}\hat{\mathbf{X}}^\ell\mathbf{C}^{\mathrm{T}}$, but the maximum amplification is given by the mode associated with the largest eigenvalue of this matrix, where $\mathbf{C}$ is the discretization of the output operators that relate $\hat{u}_\ell(y,t)$ and $\hat{w}_\ell(y,t)$ to $\hat{v}_\ell(y,t)$ and $\hat{\eta}_\ell(y,t)$. In practice, it is more efficient to exploit the structure of the problem by finding the largest singular value of $\mathbf{CR}$, where $\mathbf{R}$ is the Cholesky decomposition of $\hat{\mathbf{X}}^\ell$ in (61). The mode associated with the largest amplification is then given by the corresponding singular vector [13].

V. Results

As an initial study, the effects of including a sinusoidal riblet for the linearised flow at a Reynolds number Re = 4200 are investigated. The $u(\tilde{y}, \tilde{z})$ component of the mode associated with the maximum amplification when riblets with peak to peak separation of $2\pi/8$ and amplitude 0.15 are introduced onto the lower wall in the channel flow is shown in Fig. 3. It can be seen that in this component, the flow is raised up above the riblets and the largest component of this flow occurs in the upper half of the channel. This has the effect of reducing the flow in the lower half of the channel, which in turn, reduces the gradient of the shear stress at the riblet wall. It should be emphasised that this models the linearised flow; in practice, it is likely that the nonlinear effects will have a more important role at this Reynolds number.

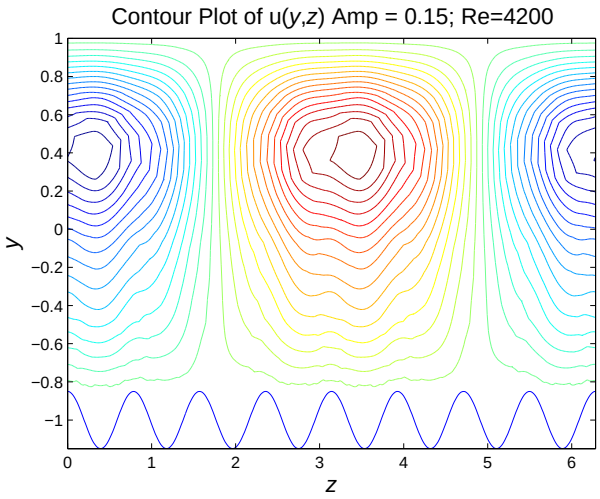

Fig. 3. Contour plot of streamwise velocity $u(\tilde{y}, \tilde{z})$ component of mode associated with maximum amplification for the case with riblets on lower wall.

VI. Conclusion

This paper has developed a linearized model of the channel flow between two plates, where one of the plates has a riblet structure. The boundary conditions associated with the riblets are transferred into the partial differential equations describing the flow by applying a transformation of coordinates. The number of components in the flow equations are reduced by restricting attention to streamwise constant variations. By expressing the model in terms of spatial Fourier components in the spanwise direction, the structure of the resulting large-scale, finite-dimensional state space model can be exploited, allowing the amplification of noise energy to be obtained by calculating the controllability gramian via a set of decoupled Lyapunov equations. The model shows that for flow at low Reynolds numbers, the inclusion of riblets reduces the maximum amplification of the noise energy and it appears that this reduction in energy amplification may be associated with the presence of counter-rotating vortices at the peaks of the riblet structures. Current work is using the model to examine the effect of riblets on the energy amplification in flows at a range of Reynolds numbers and for a range of riblet amplitudes and separations.

References

[1] M. Walsh, "Riblets as a viscous drag reduction technique," *AIAA J.*, vol. 21, pp. 485–486, 1983.

[2] ——, "Riblets," in *Viscous Drag Reduction in Boundary Layers*, D. Bushnell and J. Hefner, Eds. New York, NY: AIAA, 1990, pp. 203–261.

[3] D. Bechert, M. Bruse, W. Hage, J. van der Hoeven, and G. Hoppe, "Experiments on drag-reducing surfaces and their optimization with an adjustable geometry," *J. Fluid Mechanics*, vol. 338, pp. 59–87, 1997.

[4] E. Coustols and A. Savill, "Turbulent skin-friction drag reduction by active and passive means," in *Special Course on Skin Friction Drag Reduction*, J. Cousteix, Ed. AGARD Report 796, 1993, pp. 8–1 – 8–80.

[5] D. Bechert, M. Bruse, and W. Hage, "Experiments with three-dimensional riblets as an idealized model of shark skin," *Experiments in Fluids*, vol. 28, pp. 403–412, 2000.

[6] B. Dean and B. Bhushan, "Shark-skin surfaces for fluid-drag reduction in turbulent flow: a review," *Philosophical Transactions of the Royal Society A*, vol. 368, no. 1929, pp. 4775–4806, 2010.

[7] P. Viswanath, "Aircraft viscous drag reduction using riblets," *Progress in Aerospace Sciences*, vol. 38, pp. 571–600, 2002.

[8] J. Reneaux, "Overview on drag reduction technologies for civil transport aircraft," in *Proc. European Congress on Computational Methods in Applied Sciences and Engineering ECCOMAS*, Jyvaskyla, Finland, 2004.

[9] H. Choi, P. Moin, and J. Kim, "Direct numerical simulation of turbulent flow over riblets," *J. Fluid Mechanics*, vol. 255, pp. 503–539, 1993.

[10] D. Chu and G. Karniadakis, "A direct numerical simulation of laminar and turbulent flow over riblet-mounted surfaces," *J. Fluid Mechanics*, vol. 250, pp. 1–42, 1993.

[11] R. García-Mayoral and J. Jiménez, "Hydrodynamic stability and breakdown of the viscous regime over riblets," *J. Fluid Mechanics*, vol. 678, pp. 317–347, 2011.

[12] ——, "Drag reduction by riblets," *Philosphical Transactions of the Royal Society A*, vol. 369, no. 1940, pp. 1412–1427, 2011.

[13] S. Duncan and A. Papachristodoulou, "Energy amplification in channel flow over riblets," in *Proc. IEEE Multi-Conf. on Systems and Control*, Denver, CO, 2011, pp. 456–461.

[14] ——, "Analyzing the energy amplification in channel flow over riblets," Department of Engineering Science, University of Oxford, Oxford, UK, Tech. Rep. 2327/11, 2011.

[15] B. Bamieh and M. Dahleh, "Energy amplification in channel flows with stochastic excitation," *Physics of Fluids*, vol. 13, no. 11, pp. 3258–3268, 2001.

[16] M. Jovanovic and B. Bamieh, "Componentwise energy amplification in channel flows," *J. Fluid Mechanics*, vol. 534, pp. 145–183, 2005.

[17] J. Boyd, *Chebyshev and Fourier Spectral Methods*, 2nd ed. New York, NY: Dover, 2001.

[18] L. Trefethen, *Spectral Methods in Matlab*. Philapelphia, PA: SIAM, 2000.

[19] J. Weidman and S. Reddy, "A MATLAB differentiation matrix suite," *ACM Transactions on Mathematical Software*, vol. 26, no. 4, pp. 465–519, 2000.

[20] A. Kasliwal, "Drag reduction over aerofoils fitted with riblets," Department of Engineering Science, University of Oxford, Oxford, UK, Tech. Rep., 2012.